substrate is removed by a selective etch. The remaining processes then follow a normal HBT fabrication sequence.

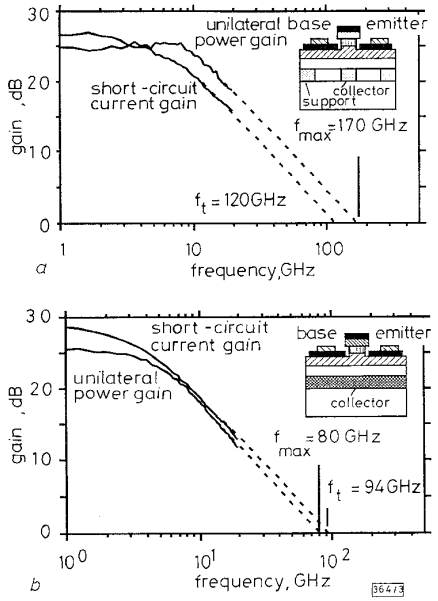

Fig. 3 *Comparison of RF characteristics of narrow collector transferred substrate HBT to wide collector transferred substrate HBT*

a Narrow *b* Wide
$J_e = 10^5 A/cm^2$
$V_{ce} = 1.2V$
1μm emitter, 11μm collector

Fig. 3 shows the RF characteristics of recently fabricated devices. It compares two kinds of devices. Fig. 3*a* has a 1μm emitter and 2μm collector fingers. Fig. 3*b* has a 1μm emitter but a large collector of the full 11μm width of the base mesa. This wide-collector device has a geometry similar to a normal HBT, and serves as a standard of comparison for the performance of the narrow collector transferred substrate HBTs. The control device exhibits f_τ = 94GHz and f_{max} = 80GHz with a β of 28, and the narrow collector transferred substrate HBT exhibits a f_τ of 120GHz and an f_{max} improved to 170GHz and a β of 20.

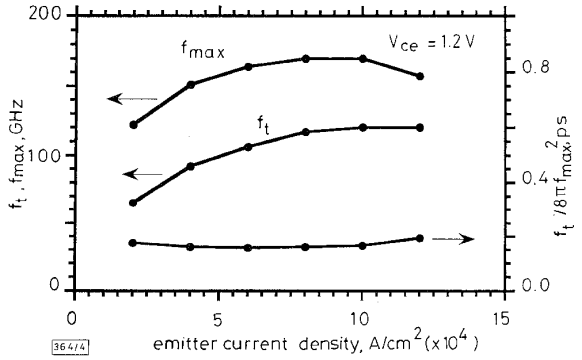

Fig. 4 *Variation of f_τ and f_{max} with emitter current density*

Fig. 4 shows the variation of f_τ, f_{max}, and the inferred collector-base time constant ($r_{bb}C_{cb}|_{inferred} = f_\tau/8\pi f_{max}^2$) with bias current for the narrow collector device. The inferred $r_{bb}C_{cb}$ increases at high currents due to the onset of base pushout.

The transferred substrate HBT is a scalable device whose f_{max} increases with submicrometre scaling. Deep submicrometre RIE etch processes are now being developed for emitter fabrication, and an improved epitaxial transfer process is being developed in which epoxy adhesive is replaced with a standard IC polymer (benzocyclobutene). With these improvements an HBT IC technology with device bandwidths near 500GHz should be realisable.

Acknowledgments: This work was supported by the AFOSR under grant F4962096-1-0019, ONR under grant N00014-95-1-0688, and the ARPA under the Thunder and Lightning program.

16 May 1996
Electronics Letters Online No: 19960898

U. Bhattacharya, L. Samoska, R. Pullela, J. Guthrie, Q. Lee, B. Agarwal, D. Mensa and M.J.W. Rodwell (*Department of Electrical and Computer Engineering, University of California, Santa Barbara, CA 93106, USA*)

References

1 LIN, W., HILL, D., CHAU, H.F., SWEDER, J., NAGLE, T., and DELANEY, J.: 'Laterally etched undercut (LEU) technique to reduce base-collector capacitances in heterojunction bipolar transistors'. Tech. Dig. 17th Annual GaAs IC Symp., San Diego, USA, October 1995, pp. 167–170

2 MATINE, N., PEBUARD, J.L., PARDO, F., TEISSIER, R., and PESSA, M.: 'Novel approach for InP-based ultrafast HBTs'. Proc. Eighth Int. Conf. Indium Phosphide and Related Materials, Schwabisch Gmund, Germany, April 1996, pp. 137–140

3 HO, M.-C., JOHNSON, R.A., HO, W.J., CHANG, M.F., and ASBECK, P.M.: 'High-performance low-base-collector capacitance AlGaAs/GaAs heterojunction bipolar transistors fabricated by deep ion implantation', *IEEE Electron Devices Lett.*, 1995, **EDL-16**, (11), pp. 512–514

4 YAMAHATA, S., KURISHIMA, K., ITO, H., MATSUOKA, Y., and : 'Over-220-GHz-f_T-and f_{max} InP/InGaAs double heterojunction bipolar transistors with a new hexagonal shaped emitter'. Tech. Dig. 17th Annual GaAs IC Symp., San Diego, USA, October 1995, pp. 163–166

5 BHATTACHARYA, U., MONDRY, M.J., HURTZ, G., TAN, I-H., PULLELA, R., REDDY, M., GUTHRIE, J., RODWELL, M.J.W., and BOWERS, J.E.: 'Transferred substrate Schottky-collector heterojunction bipolar transistors: first results and scaling laws for high f_{max}', *IEEE Electron Device Lett.*, 1995, **EDL-16**, (8), pp. 357–359

6 BHATTACHARYA, U., MONDRY, M.J., HURTZ, G., GUTHRIE, J., and RODWELL, M.J.W.: '100GHz Transferred substrate Schottky-collector heterojunction bipolar transistor'. Proc. Eighth Int. Conf. Indium Phosphide and Related Materials, Schwabisch Gmund, April 1996, Germany, pp. 145–148

Buried refractive microlenses formed by selective oxidation of AlGaAs

O. Blum, K.L. Lear, H.Q. Hou and M.E. Warren

Indexing terms: Aluminium gallium arsenide, Oxidation

The authors demonstrate a novel method of fabricating buried refractive microlenses formed by selective oxidation of AlGaAs epitaxial layers on a GaAs substrate. By appropriate tailoring of the Al mole fraction in the vertical direction, a lens-shaped oxidation shape was achieved. Performance of the microlenses formed in this way was experimentally evaluated at 980nm, and modelled theoretically.

Selective oxidation of AlGaAs compounds allows formation of Al_2O_3 layers embedded in unoxidised semiconductor material [1]. It is known that the oxidation rate depends very strongly on the Al concentration [2]. The Al composition of epitaxial $Al_xGa_{1-x}As$ layers can be vertically tailored such that selective oxidation from the side of the exposed mesa results in an oxide-semiconductor interface of a desired shape. In this way optical elements, such as refractive microlenses, can be formed. Such elements can be fabricated inside or outside cavities of a variety of microcavity structures, such as vertical cavity surface emitting lasers (VCSELs), asymmetric Fabry-Perot (ASFP) modulators, resonant cavity light emitting devices (RCLEDs), and resonant cavity photodetectors. While the benefits of integrated microlenses formed outside the VCSEL microcavity have already been demonstrated [3], the incorporation of intracavity focusing elements could result in novel cavity phenomena and further improvements in device performance. We demonstrate the formation of buried, convex lenses fabricated using the selective oxidation method.

Two micrometre AlGaAs layers with Al composition varying linearly from 98% to 90% from top to bottom are grown using metal-organic chemical vapour deposition (MOCVD) on GaAs substrates, and protected with a 100 nm GaAs cap. In sample *A*, the Al composition is varied continuously, in a linear fashion, whereas in sample *B*, Al composition is varied discretely. The linear variation is approximated by 41 AlGaAs layers of 45nm each, separated by 5 nm GaAs barriers. The Al composition is increased by 0.2% in each successive AlGaAs layer, from 90% at the substrate to 98% at the cap. Fig. 1*a* and *b* illustrates the Al mole fraction distribution in samples *A* and *B*, respectively.

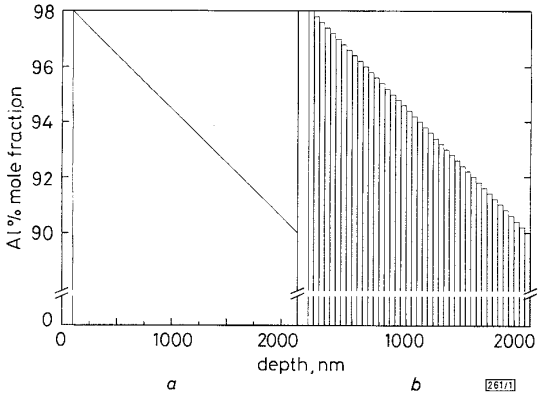

Fig. 1 *Al mole fraction against depth*
a In sample *A*, *b* In sample *B*

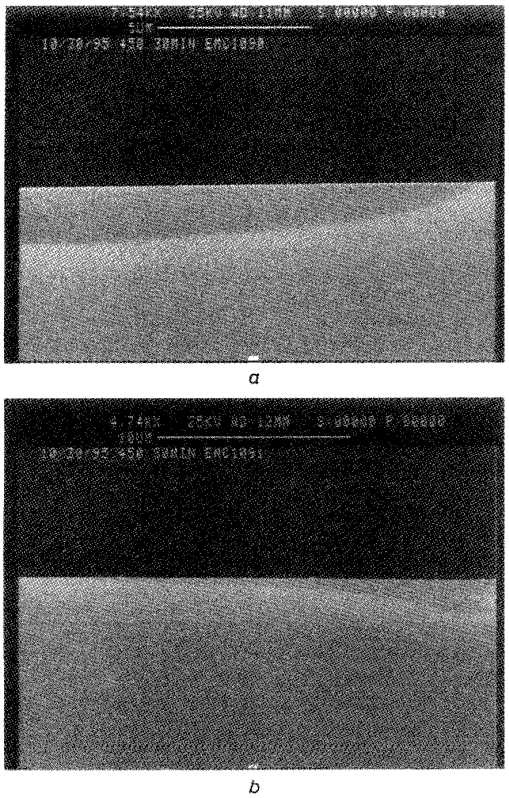

Fig. 2 *Cross-sectional SEM of partially oxidised samples*
a Sample *A* with continuous Al mole fraction grade
b Sample *B* with a digital Al grade
Dark areas are the oxidised regions, light areas are the unoxidised regions

Processing consisted of photolithographic definition and reactive ion etching of 2 to 200μm mesa stripes. Samples were then immediately oxidised in an open tube furnace held at a variety of temperatures (400°C < T < 450°C) for different times (90mm > t > 30 mm) while bubbling N_2 through water heated to 85°C.

Fig. 2*a* and *b* shows cross-sectional scanning electron microscopy (SEM) micrographs of partially oxidised mesa stripes, of samples *A* and *B*, respectively. Dark regions correspond to the oxidised material and lighter regions to the unoxidised AlGaAs and GaAs substrate. Clearly, drastically different oxidation front shapes are obtained with the continuous Al grade (sample *A*) and the discrete Al grade (sample *B*). In spite of, nominally, the same variation of the Al mole fraction, sample *A* is not suitable for formation of convex refractive lenses, whereas sample *B* is. Thus the shape of the oxidation front is determined not only by the variation of the Al mole fraction, but also by its distribution. We speculate that this drastic difference in the shape of the oxidation front can be attributed to the 2-D nature of the oxidation process in the bulk material. By separating the individual AlGaAs layers with GaAs barriers, vertical contributions to the total rate of oxidation can be decreased, while the lateral contributions to the rate of oxidation remain unaffected, resulting in a different oxide front shape. Further investigation of this phenomenon is underway and will be discussed in greater detail elsewhere.

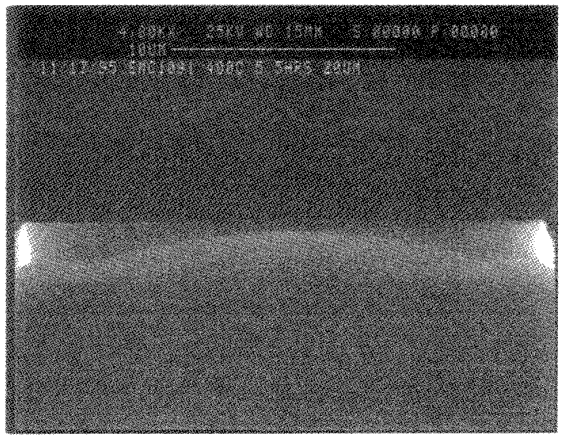

Fig. 3 *Cross-sectional SEM of lens formed by lateral oxidation of sample B (digitally graded Al mole fraction)*

Fig. 3 shows a cross-sectional SEM micrograph of a 25μm stripe of sample *B* oxidised to completion to produce a cylindrical, refractive microlens from the unoxidised AlGaAs/GaAs surrounded by the oxidised material. This sample was oxidised at 400°C for 5.5h. Assuming that the GaAs barriers remain unoxidised, the refractive index (n) in the oxidised area is calculated to be 1.7, while the refractive index in the unoxidised area is 3.05. Theses values were found using the effective index approximation and assuming that the Al-oxide, AlGaAs and GaAs layers have n of 1.5, 3.0 and 3.5, respectively.

At 980nm, the average focal length of the lenses, of the same sise as shown in Fig. 2, was measured to be 16.3μm in air, and calculated to be 17μm. The theoretical value of the focal length was obtained from simulation with commercial ray tracing software, using the digitised lens profile from the SEM as the input. The lens diameter was measured at 17μm, resulting in a numerical aperture of 0.52.

We also oxidised 50μm stripes and measured average focal lengths of 121μm, with the calculated focal length of 111μm. The lens diameter was found to be 43μm, and thus the numerical aperture for this lens was 0.18. The better agreement between calculated and measured focal lengths for the 25μm lenses can be attributed to their closer approximation of the quadratic shape assumed in our model. Although circular lenses were also fabricated and their focal lengths measured, digitised lens profiles were only measured for cylindrical lenses due to the difficulty of accurately cleaving along the circular lens diameter. Consequently, comparisons of the experimental and theoretical focal length were only performed for the cylindrical lenses. We have investigated theoretically and experimentally the spatial dependence of the oxidation front on the Al mole fraction. Lens elements were formed, their curvatures confirmed by SEM of the cross-sections, and their optical properties, such as focal length, measured. Such elements can be integrated into active devices and should improve device performance.

6 May 1996
Electronics Letters Online No: 19960887

O. Blum, K.L. Lear, H.Q. Hou and M.E. Warren (*Department 1312, MS0603, Sandia National Laboratories, Albuquerque, NM, USA*)

References

1 DALLESASSE, J.M., HOLONYAK, N. Jr., SUGG, A.R., RICHARD, T.A., and EL-ZEIN, N.: 'Hydrolyzation oxidation of $Al_xGa_{1-x}As$-AlAs-GaAs quantum well heterostructures and superlattices', *Appl. Phys. Lett.*, 1990, **57**, pp. 2844–2846

2 CHOQUETTE, K.D., SCHNEIDER, R.P. Jr., LEAR, K.L., and GEIB, K.M.: 'Low threshold voltage vertical-cavity lasers fabricated by selective oxidation', *Electron. Lett.*, 1994, **30**, pp. 2043–2044

3 BLUM, O., KILCOYNE, S.P., WARREN, M.E., DU, T.C., LEAR, K.L., SCHNEIDER, R.P. Jr., CARSON, R.F., ROBINSON, G., and PETERS, F.H.: 'Vertical-cavity surface-emitting lasers with integrated refractive microlenses', *Electron. Lett.*, 1995, **31**, pp. 44–45

Comparison of dry etch techniques for GaN

R.J. Shul, G.B. McClellan, S.J. Pearton,
C.R. Abernathy, C. Constantine and C. Barratt

Indexing terms: Gallium nitride, Etching

Dry etching of GaN in $Cl_2/H_2/CH_4/Ar$ has been compared using electron cyclotron resonance (ECR), inductively coupled plasma (ICP), and reactive ion etch (RIE) systems. GaN etch rates and surface morphology were obtained as a function of RF power, and showed significant improvements under high density plasma conditions.

Introduction: Device demonstrations of blue, green, and ultraviolet emitters and detectors, and high temperature electronics, continue to increase interest in the wide bandgap group-III nitrides [1–3]. Realisation of more advanced devices, including lasers, requires dry etch processes which are well controlled, smooth, highly anisotropic, and have etch rates exceeding 0.5μm/min.

Anisotropic GaN etching has been reported in reactive ion etch (RIE) systems with etch rates approaching 600Å/min owing to the acceleration of energetic ions from the plasma to the wafer [4]. This energetic ion bombardment can damage the sample and degrade both electrical and optical device performance. Therefore, a great deal of interest has been generated in low damage etch processes based on high density electron cyclotron resonance (ECR) plasmas and inductively coupled plasmas (ICP). Owing to the magnetic confinement of electrons in the microwave source, high density ECR plasmas are formed at low pressures with low plasma potentials and ion energies. High density ICP plasmas are formed in a dielectric vessel encircled by an inductive coil into which RF power is applied. A strong magnetic field is induced in the centre of the chamber which generates a high density plasma owing to the circular region of the electric field that exists concentric to the coil. At low pressures, the plasma diffuses from the generation region and drifts to the substrate at relatively low ion energy. Less damage than that produced by RIE plasmas is therefore expected during ECR and ICP etching, and much higher etch rates should be achieved with the high density sources.

Experiment: The GaN films were grown by metal organic molecular beam epitaxy (MO-MBE) [5]. The plasma reactor used in this study was a load-locked Plasma-Therm SLR 770 etch system operating in either an ECR, ICP, or RIE mode. The ECR plasma was formed with a low profile 2.45GHz Astex 4400 ECR source (1000W power) in which the upper magnet was operated at 165A. To minimise field divergence and to optimise plasma uniformity and ion density across the chamber, a lower external secondary collimating magnet was run at 25A. The RIE plasma was generated using a 13.56MHz RF power supply. The ICP plasma was formed by replacing the ECR source with a Plasma-Therm 2MHz ICP source operating at 500W RF power. In the ECR and ICP, energetic ion bombardment was provided by superimposing an RF bias (13.56MHz) on the sample. Unless otherwise mentioned, plasma etch parameters used in this study were: 10sccm of Cl_2, 15sccm of H_2, 10sccm of Ar, 3sccm of CH_4, 25°C electrode temperature, and 1mtorr total pressure. For the ECR and ICP, the RF power ranged from 1 to 450W with corresponding DC biases of –10 to –400 ± 25V. RIE RF powers ranged from 50 to 450W with corresponding DC biases of –270 to –950 ± 50V.

All samples were patterned with AZ-4330 photoresist and mounted using vacuum grease on an anodised Al carrier that was clamped to the cathode and cooled with He. Etch rates were calculated from the depth of etched features measured with a Dektak stylus profilometer after the photoresist was removed. Each sample was approximately 1cm², and depth measurements were taken at a minimum of three positions. Standard deviation of the etch depth across the sample was nominally < ± 15% with run-to-run variation < ± 10%. Root-mean-square (RMS) surface roughness was quantified using a Digital Instruments Dimension 3000 atomic force microscope (AFM) system.

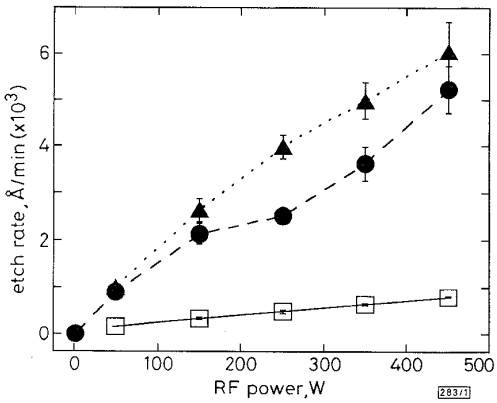

Fig. 1 *GaN etch rates against RF power in ECR-, RIE-, and ICP-generated $Cl_2/H_2/CH_4/Ar$ plasma*

● ECR
□ RIE
▲ ICP

Results and discussion: GaN etch rates are shown in Fig. 1 against RF power for the three plasmas. The lowest RF power required to generate a stable RIE plasma was 50W, whereas the ECR and ICP plasmas were stable at 1W RF power. At constant pressure, the DC bias was much higher in the RIE since the ion densities were so much lower. The GaN etch rates increased as a function of RF power independent of etch technique owing to enhanced sputter desorption of the etch products. The GaN etch rates obtained in the ICP were 10 to 50% faster than those from the ECR. Since the DC bias was similar as a function RF power, higher etch rates in the ICP were attributed to higher concentrations of reactive neutrals. The ECR and ICP GaN etch rates were ~5–10 times faster than those obtained in the RIE owing to higher plasma densities generated in the ECR and ICP.

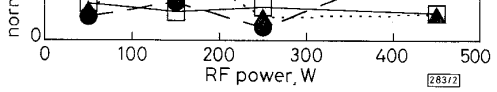

Fig. 2 *GaN RMS surface roughness normalised to RMS roughness of as-grown GaN against RF power in ECR-, RIE- and ICP-generated $Cl_2/H_2/CH_4/Ar$ plasma*

● ECR
□ RIE
▲ ICP

The RMS roughness for samples exposed to the plasmas were quantified using AFM, and normalised to the RMS roughness for the as-grown samples. The RMS values for as-grown GaN were 65.2nm for samples etched in the ICP and 19.3nm for samples